

MOMENT-ROTATION HYSTERESIS BEHAVIOR OF TOP AND SEAT ANGLE STEEL FRAME CONNECTIONS

By Anant R. Kukreti,¹ Member, ASCE, and Ali S. Abolmaali²

ABSTRACT: This paper presents an approach toward formulating analytical models to predict the moment-rotation hysteresis behavior of top and seat angle connections. Experimental results obtained from 12 top and seat angle connection specimens are used to obtain the prediction equations for the parameters defining the moment rotation hysteresis loops of a typical top and seat angle connection. These parameters include the initial stiffness, ultimate moment capacity, ultimate rotation, the transition moment, characteristic moment, and rigidity parameter. Regression analysis results and comparisons with test results are presented to demonstrate the acceptability of these prediction equations. The prediction equations obtained for these parameters are used to develop four different moment rotation hysteresis models for the connection: the bilinear, elastoplastic, Ramberg-Osgood, and modified bilinear models. The results of the study show that the top and seat angle connection behaves as a semirigid connection. A wide range of initial stiffnesses and ultimate moment capacities are possible to achieve by altering the connection geometry related variables within a practical range. For certain geometric configurations of the connection, significant transfer of moment from the beam to the column can occur before the connection fails. Also, it is possible to design a connection with flow stiffness and small moment transfer capability, so that it behaves in a manner such that it is close to being classified as a pin connection. The prediction equations developed for the parameters characterizing the four hysteresis models give acceptable results when compared to experimental results. The degree to which the models idealize the actual behavior varies with the elastoplastic model being the least conservative and the modified bilinear model being the best. The Ramberg-Osgood model is the most accurate in just modeling the nonpinching moment-rotation loops.

INTRODUCTION

This paper represents an approach toward formulating analytical models to predict the moment-rotation hysteresis behavior of top and seat angle connections, which are commonly used in the design of steel frame structures. These analytical models idealize the actual observed moment-rotation hysteresis behavior to a varying degree of complexity and prediction capability. The American Institute of Steel Construction, in its load and resistance factor design (LRFD) *Manual of steel construction* (1994), suggested a design procedure for this connection, in which the seat angle is assumed to transfer only vertical shear force, and no significant moment is assumed to be transferred by the beam end. The top angle is solely used for lateral stability in this design, and is not considered to carry any gravity load. However, according to the experiments conducted by Rathbun (1936) and Hechtman and Johnston (1947), it was reported that top and seat angle connections will resist some end moment of the beam, and therefore can be classified as partially constrained connections or semirigid connections. Most of the studies reported for top and seat connections present experimental results and analytical models characterizing the moment-rotation ($M-\theta$) behavior under statically increasing monotonic loads. A three-parameter exponential model is proposed by Kishi and Chen (1986, 1987a,b). Marley and Gerstle (1982) reported results of a total of 26 tests. The moment-rotation curves were obtained from extrapolation of the test results from the case of cyclic loading to the case of a monotonically increasing moment versus rotation relationship. Since not all connection parameters were varied in these tests, no generalized moment-rotation model was developed from these

test results to characterize the cyclic behavior of the connection. However, Marley and Gerstle (1982) did conclude that the moment-rotation behavior of the connection cannot be ignored in the analysis. Driscoll and Lu (1989) reported results for six full-scale tests of large top and seat angle connections, in which the number of bolt rows, angle thickness, and bolt pretension were varied. All test specimens were cyclically loaded in a statical fashion, which was not truly cyclic, to determine load reversal effects. It is reported that the snug-tight connection for the multiple row of bolts behaved stiffer and stronger than its fully pretensioned counterpart. The snug-tight connection also reacted less adversely to load reversal, and its load-deformation response remained linear over a large range of loading.

Earlier studies on cyclic behavior of steel frame connections included investigations on cyclic behavior of fully welded connections, with and without web angles to transmit shear, and end-plate connections (Popov and Pinkey 1968; Popov and Bertero 1973; Popov et al. 1985; Lee and Lu 1988; Tsai 1988; Tsai and Popov 1990; Biolzi 1982). Popov and Pinkey (1968) used Ramberg-Osgood functions in modeling hysteresis loops obtained by using such models to be in close agreement with the experimental loops of nonslip specimens. Popov and Bertero (1973) suggested a skew-symmetric moment-rotation model for connections made by direct welding of flanges with or without connection plates.

It is accepted that certain semirigid connections can be designed to be well suited for seismically induced loads, and that they possess high ductility and energy dissipation capacities. Recent increasing interest in the use of semirigid connections for steel buildings is primarily due to the fact that potential economies can be realized by adjusting the connection stiffness to optimize the distribution of moments in the connected members. Astaneh-Asl et al. (1989) investigated the cyclic behavior of double web connections welded to a beam web and bolted to a column flange. In their study, moment rotation hysteresis loops are presented, and it was concluded that considerable moment can be resisted by these connections. Mander et al. (1994) investigated the low cycle fatigue behavior of the top and seat angle connections by applying a constant amplitude reverse cyclic load on specimens of the same geometrical properties. Their study showed that plastic moment

¹Samuel Roberts Noble Found. Presidential Prof. and Acting Dir., School of Civ. Engrg. and Envir. Sci., Univ. of Oklahoma, Norman, OK 73019.

²Grad. Res. Asst., School of Civ. Engrg. and Envir. Sci., Univ. of Oklahoma, Norman, OK.

Note. Associate Editor: C. Dale Buckner. Discussion open until January 1, 2000. To extend the closing date one month, a written request must be filed with the ASCE Manager of Journals. The manuscript for this paper was submitted for review and possible publication on April 1, 1998. This paper is part of the *Journal of Structural Engineering*, Vol. 125, No. 8, August, 1999. ©ASCE, ISSN 0733-9445/99/0008-0810-0820/\$8.00 + \$.50 per page. Paper No. 18037.

capacity and connection stiffness were sensitive to how the bolts and nuts were oriented when tightened. The seismic fatigue ratio limited plastic rotation is suggested on the order of 3%. Tsai et al. (1995) investigated the performance of 10 cyclic beam-to-wide-flange-column moment connections. The connections were bolted-web-welded-flange. Their study concluded that supplemental web welds, but not supplemental web bolts, significantly enhance the strength, ductility, and energy absorbing capacity of the connection. Experimental results indicate that the cyclic rotational capacity of this type of connection ranges from 0.009 to 0.018 rad. Vayas et al. (1995) conducted 13 experiments to investigate the cyclic behavior of beam-to-column joints of steel frames made up of welded plate members and with slender joint panels in the connection region. The performance of connections with respect to the degree of rigidity and low cyclic fatigue were examined. The behavior of the joint is divided into three actions: shear buckling of the panel, tension field action, and the frame action. Their study concluded that good performance can be achieved by properly selecting the dimensions of the web panel and surrounding flanges of the frame members. Nader and Astaneh-Asl (1996) reported shaking table tests of top and seat angle connections, with additional web angles, and the results of these tests were compared with rigid and flexible connections tested on the shaking table. Their study reports that "a well-proportioned semirigid connection designed to behave in a more ductile manner can effectively participate in the non-linear behavior of the structure, thus providing additional global structural ductility." Sarraf and Bruneau (1996) conducted cyclic testing of riveted stiffened seat angle connections taken from an 83-year-old building, and actual hysteresis behavior and potential moment resistance were investigated. It was concluded that connections can develop considerable moment resistance, but due to pinching present in hysteresis loops, low energy dissipating capacity was observed. Two analytical models are suggested to predict the capacity of this connection, and two seismic retrofit strategies are suggested.

In the present paper, first, the experimental program conducted to collect the data to develop the moment-rotation hysteresis models for top and seat connections is described, and test results for sample cases are presented. Second, the pertinent parameters for four models that can be used to analytically idealize the actual observed moment-rotation hysteresis behavior to a varying degree of accuracy are identified and presented. Third, the prediction equations obtained for these parameters by regressing the test results are presented, and are validated by comparing predicted results with those obtained from tests. Fourth, the results obtained from the four hysteresis models, which use the prediction equations for the parameters, are compared with those obtained from tests to show the levels of approximations achieved by each model.

EXPERIMENTAL PROGRAM

Test Cases Selected

The all-bolted top and seat angle connection consists of a top and a seat angle bolted to beam flanges as well as the column flange, as shown in Fig. 1. As shown in this figure, the variables defining these connections are: g_c , the distance from the heel of the angle to the centerline of the first row of bolts in the column flange; d_b , the bolt diameter; d , the depth of the beam; t , the angle thickness; l_v , the length of the angle leg (vertical) of the top or seat angle connected to the column flange; g_b , the bolt gauges in the outstanding leg of the top or seat angle; and l , the width of the top or seat angle. The range of variation of the geometric variables considered in the present study was established based on current design and fabrication practices followed by the steel industry and the Amer-

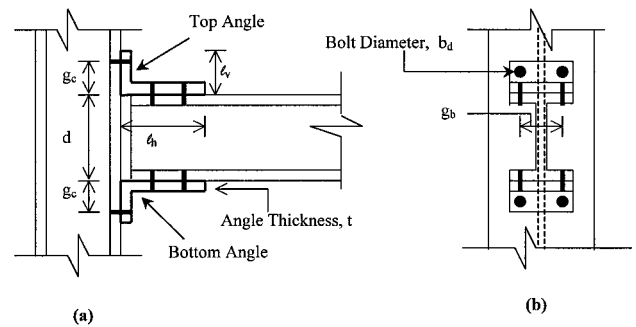


FIG. 1. Geometric Variables for Top and Seat Angle Connection: (a) Front View; (b) Side View

ican Institute of Steel Construction (LRFD Manual 1994). The testing program was limited to 12 test cases. The values of the geometric variables for these 12 cases selected and the nomenclature adopted to designate each case are presented in the second column of Table 1. In this column, TS stands for top and seat angle connection, l_h is the length of the angle leg (horizontal) of the top or seat angle connected to the beam flange, and the variables l_v , t , d_b , g_c , and d mean the same as defined earlier. All these geometric variables are expressed in millimeters in the present study. The corresponding values and test designations in inch units are also indicated in Table 1.

Typical Test Specimen

A typical test specimen used in the study consisted of a beam connected to a short column by means of the top and seat angle connections, as shown in Fig. 2. As shown in this figure, two bolt rows are used in the angle leg connected to the beam flange, and one bolt row is used in the outstanding angle leg connected to the column flange. The column used in all specimens was a W200 × 100 (W8 × 67) short column, 1,372 mm (54 in.) in length, which was bolted to the column of the reaction test frame. A column with a large flange thickness [=24 mm (15/16 in.)] was selected to ensure that the column deformations would not add significant rotation to the overall rotation of the connection. This permitted the same column section to be reused for all tests. The writers are aware that this limits the scope of the study, since column deformations may play a major role in beam-to-column connection behavior. Also, until rational procedures based on tests are available to understand how much the column deformations contribute to total connection rotation, this limitation was imposed as a first step toward the study. The writers are studying this aspect, and the results will be presented later. However, they believe that this is a first step toward developing the constitutive relationship (i.e., the $M-\theta$ relationship) of the connection that can be incorporated in a frame analysis computer program in which the semirigid connections are modeled as moment springs. Such constitutive relationships for cyclic behavior of semirigid connections are not currently available in the literature. Other researchers, for example, Astaneh-Asl et al. (1989), have also used this approach to investigate the moment-rotation hysteresis behavior of steel connections.

Two different beam depths are used, as indicated in Table 1. The beam sections used to obtain these beam depths are W360 × 64 (W14 × 43) and W410 × 67 (W16 × 45). Each beam was of 978 mm (38.5 in.) length. These two beams are selected to ensure a variation in the depth of the beam, and the beam sizes are selected such that no beam element yields during testing. This ensured that inelastic (yielding) behavior, if any, would occur only in the connection elements, which consist of the two angle legs and bolts. This permitted the

TABLE 1. Summary of Stiffness and Moment Capacity Results

Test number (1)	Test designation $TS - l_h \times l_v \times t \times d_b - g_c - d$ [mm (in.)] (2)	Yield stress of angle material MPa (ksi) (3)	Initial stiffness kN·m/rad (kip-in./rad) (4)	Failure Results			Pinching (8)
				M_u kN·m (kip-in.) (5)	Rotation (rad) (6)	Mode (7)	
1	$TS - 152 \times 102 \times 19 - 16 - 64 - 360$ ($TS - 6 \times 4 \times 3/4 - 5/8 - 2.5 - 14$)	324 (47)	27,193 (247,063)	89 (791)	0.023	Bolt failure	Moderate
2	$TS - 152 \times 152 \times 9.5 - 16 - 114 - 360$ ($TS - 6 \times 6 \times 3/8 - 5/8 - 4.5 - 14$)	338 (49)	8,248 (73,000)	25 (219)	0.045	Excessive rotation ^a	None
3	$TS - 152 \times 152 \times 19 - 16 - 90 - 360$ ($TS - 6 \times 6 \times 3/4 - 5/8 - 3.5 - 14$)	345 (50)	19,063 (168,732)	95 (840)	0.042	Bolt failure	Significant
4	$TS - 152 \times 152 \times 19 - 16 - 114 - 400$ ($TS - 6 \times 6 \times 3/4 - 5/8 - 4.5 - 16$)	345 (50)	20,068 (177,621)	84 (745)	0.045	Excessive rotation	Significant
5	$TS - 152 \times 102 \times 19 - 19 - 64 - 360$ ($TS - 6 \times 4 \times 3/4 - 3/4 - 2.5 - 14$)	324 (47)	48,445 (428,796)	138 (1,221)	0.034	Bolt failure	Significant
6	$TS - 152 \times 102 \times 12.7 - 19 - 64 - 360$ ($TS - 6 \times 4 \times 1/2 - 3/4 - 2.5 - 14$)	352 (51)	21,831 (193,226)	92 (813)	0.045	Excessive rotation	Little
7 ^b	$TS - 152 \times 152 \times 19 - 19 - 64 - 400$ ($TS - 6 \times 4 \times 3/4 - 3/4 - 2.5 - 16$)	352 (51)	79,936 (707,523)	146 (1,296)	0.023	Bolt failure	Significant
8	$TS - 152 \times 102 \times 12.7 - 19 - 64 - 400$ ($TS - 6 \times 4 \times 1/2 - 3/4 - 2.5 - 16$)	345 (50)	60,238 (533,178)	102 (901)	0.045	Excessive rotation	Little
9	$TS - 152 \times 152 \times 19 - 19 - 90 - 400$ ($TS - 6 \times 6 \times 3/4 - 3/4 - 3.5 - 16$)	324 (47)	27,098 (239,845)	132 (1,164)	0.044	Bolt failure	Moderate
10	$TS - 152 \times 102 \times 19 - 22 - 64 - 400$ ($TS - 6 \times 4 \times 3/4 - 7/8 - 2.5 - 16$)	345 (50)	68,057 (602,379)	188 (1,665)	0.038	Bolt failure	Significant
11	$TS - 152 \times 152 \times 19 - 22 - 64 - 400$ ($TS - 6 \times 6 \times 3/4 - 7/8 - 2.5 - 16$)	345 (50)	71,089 (629,219)	202 (1,792)	0.045	Excessive rotation	Significant
12	$TS - 152 \times 152 \times 19 - 22 - 114 - 400$ ($TS - 6 \times 6 \times 3/4 - 7/8 - 4.5 - 16$)	338 (49)	21,481 (190,132)	104 (920)	0.045	Excessive rotation	Moderate

^aFailure due to excessive rotation was $\theta = 0.045$ rad.

^bValues for K , and θ , for test 7 were not meaningful.

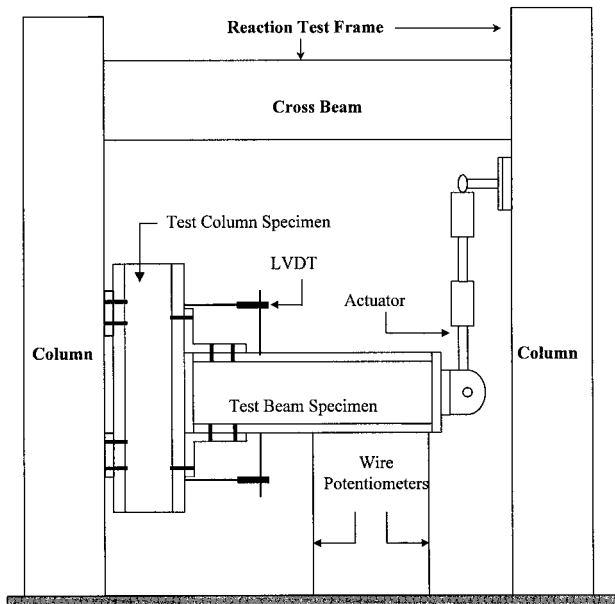


FIG. 2. Typical Test Setup and Instrumentation

development of the constitutive relationship (i.e., the $M-\theta$ relationship) for the connection alone until its failure. From Table 1, it can be seen that the following two types of angles are used: $L152 \times 152 \times t$ ($L6 \times 6 \times t$) and $L152 \times 102 \times t$ ($L6 \times 4 \times t$), where the angle thickness, t , was varied from a low value of 9.5 mm (3/8 in.) to a high value of 19 mm (3/4 in.), and with an intermediate value of 12.7 mm (1/2 in.). A325 high-strength bolts were used in all of the experiments, with bolt diameters of 16 mm (5/8 in.), 19 mm (3/4 in.), and 22 mm (7/8 in.). A torque wrench was used to tighten the bolts. All of the A325 bolts were tightened to develop a pretension force equal to their proof load.

Test Setup and Instrumentation

The total test setup and instrumentation used in the present study are shown in Fig. 2. This setup, which was used for all of the test specimens, consists of (1) an actuator to apply the force; (2) a beam of a reaction frame to support the actuator; and (3) a column of a reaction frame to support the column in the test specimen. The whole reaction frame was bolted to the laboratory floor, and the column of the test specimen was connected to the column of the reaction frame by means of four 25 mm (1 in.) diameter high-strength A325 bolts. Lateral braces were provided at the beam end connected to the actuator swivel to prevent out-of-plane buckling of the test specimen. The instrumentation consisted of two linear variable displacement transducers (LVDTs) to calculate the relative connection rotation, two wire potentiometers to measure displacements at two points along the beam specimen span, and strain gauged bolts to measure bolt forces. In addition, the actuator had a load cell and displacement transducers installed in it to measure the cyclic load applied to the beam end and the actuator stroke (displacement), respectively. The two LVDTs were placed on the top and bottom flanges of the beam using magnetic bases such that the LVDT tips touched the connection column flange just above the connection top and bottom seat angles. Thus, the relative displacements of the two LVDTs divided by the vertical distance between the two LVDT tips gives the local rotation of the connection. The global rotation of the connection was also calculated by dividing the vertical displacement recorded by each wire potentiometer by the distance of the wire potentiometer from the face of the specimen column flange. Hence, the connection rotation at every load level was measured in two independent ways: using the LVDT readings and the wire potentiometer readings. The moment on the connection was calculated by multiplying the force recorded by the actuator load cell by the distance from the centerline of the actuator to the face of the column. This distance was measured to be 1,130 mm (44.5 in.). The bolt

forces were calculated from the strains measured by specially placed bolt gauges inside holes drilled into the bolt shanks. However, the bolt force results are not presented in the current paper, since they were not used in the development of the moment-rotation models for the connection.

Loading History

The specimen was first loaded to a 4.45 kN (1 kip) load applied by the actuator in tension. Then the specimen was unloaded and reverse loading was applied to a negative value of 4.45 kN (1 kip) actuator load in compression, and was finally reloaded to zero. This process was defined as the 4.45 kN (1 kip) loop. For each specimen, three cycles of such loop were applied at the beginning of the test. For the beginning few cycles, the load was incremented in 4.45 kN (1 kip) increments to force the connection elements to remain elastic. This was required to compute the value of the initial stiffness, K_i , from the moment-rotation history recorded for these elastic cycles. Next, the specimen was subjected to three cycles of 8.9 kN (2 kip) loops. The third load step consisted of applying three cycles of 13.35 kN (3 kip) loops, followed by two cycles of 17.8 kN (4 kip) loops. This process was repeated during the early stages of the test, and during this stage load control was used to increment the cyclic load. The load control was continued until there was a significant difference in the rotation at peak values in tension and compression. At this point, the control was switched to displacement control, and the displacement was incremented at 2.5 mm (0.1 in.) intervals. The reading of the wire transducer connected to the beam end, which was bolted to the actuator swivel, was used to apply 2.5 mm (0.1 in.) increments in displacement of the beam end. The small value of 2.5 mm (0.1 in.) was selected to ensure that, due to the switch from load to displacement control, no sudden jump occurs. This increment of 2.5 mm (0.1 in.) was continued until a 25 mm (1 in.) displacement value was reached, then the increment was changed to 5 mm (0.2 in.). This displacement increment was continued until either bolt failure occurred or excessive connection rotation was noticed.

Testing Procedure

The same testing procedure was followed for all of the test specimens. Each specimen was assembled with all of the bolts

tightened to their proof load. Next, whitewash was applied to the connection region to detect yielding in the different components of the connection. The previously calibrated LVDTs were placed on the top and bottom flange of the beam, and the two wire potentiometers, which were also previously calibrated, were installed. The actuator was then bolted to the beam using four 19 mm (3/4 in.) A325 bolts. The LVDTs, wire potentiometers, actuator load, and displacement transducers were connected to an automated data acquisition system to record and process the data, and the whole experiment was computer controlled. After the bolts were tightened and the actuator was connected, the cyclic loading was applied through the actuator, following the loading history described in the previous section, until either bolt failure or excessive rotation occurred. The connection rotation and moment were recorded as the test continued.

TEST RESULTS

The moment-rotation hysteresis loops obtained for four tests are presented in Fig. 3. Only results for four representative tests are presented, which cover a test with low K_i and M_u (test 2: $K_i = 8,248 \text{ kN}\cdot\text{m}/\text{rad}$, $M_u = 25 \text{ kN}\cdot\text{m}$), a test with high K_i and M_u (test 11: $K_i = 71,089 \text{ kN}\cdot\text{m}/\text{rad}$, $M_u = 202 \text{ kN}\cdot\text{m}$), and two tests with values in between (test 6: $K_i = 21,831 \text{ kN}\cdot\text{m}/\text{rad}$, $M_u = 92 \text{ kN}\cdot\text{m}$; test 5: $K_i = 48,445 \text{ kN}\cdot\text{m}/\text{rad}$, $M_u = 138 \text{ kN}\cdot\text{m}$). In the testing, failure of the connection was observed to occur due to either bolt failure (rupture) in tension or excessive rotation of the connection. This excessive or ultimate rotation (θ_u) was found to be 0.045 rad; the test cases that failed in this mode corresponded to a separation at the heel of the top or bottom angle from the column flange of about 38 mm (1.5 in.). It was found that when excessive rotation occurs, significant loss in stiffness of the connection occurs due to excessive yielding of the angle legs. Then, the gain in moment (i.e., strength) in subsequent load cycles is very small. The failure in tests 1, 3, 5, 7, 9, and 10 was observed to be bolt failure, whereas in tests 2, 4, 6, 8, 11, and 12 failure occurred due to excessive rotation. The test values obtained for initial stiffness, ultimate moment capacity, and ultimate rotation for all 12 tests are presented in Table 1. All of the test cases, except for test 2 [TS152 × 152 × 19 – 16 – 64 – 360 (TS – 6 × 6 × 3/8 – 5/8 – 4.5 – 14)], exhibited

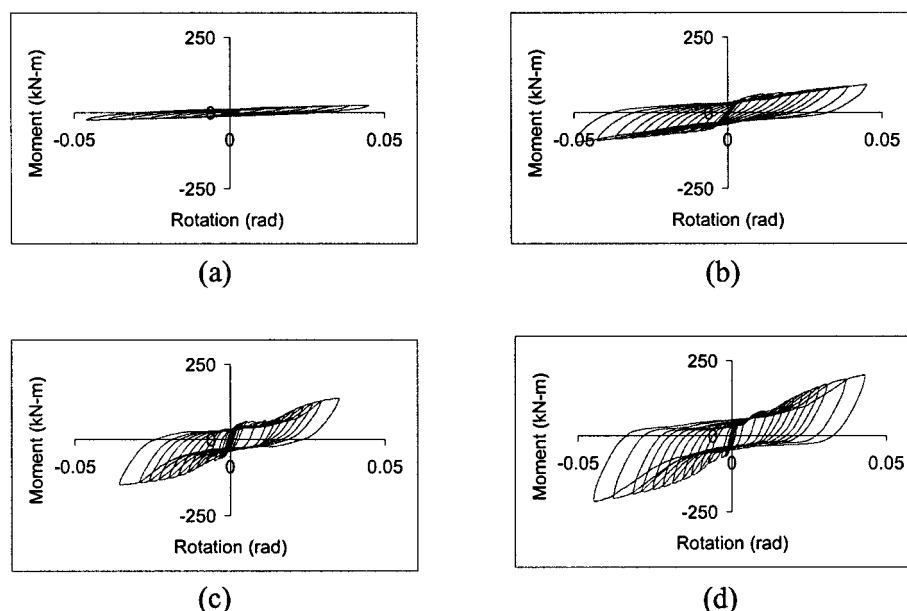


FIG. 3. Experimental Moment-Rotation Hysteresis Loops Obtained: (a) Test 2: TS – 152 × 102 × 9.5 – 16 – 64 – 360; (b) Test 6: TS – 152 × 102 × 12.7 – 19 – 64 – 360; (c) Test 5: TS – 152 × 102 × 19 – 19 – 64 – 360; (d) Test 11: TS – 152 × 152 × 19 – 22 – 114 – 400

TABLE 2. Comparison of Test Results

Variable (1)	Test compared (2)	Initial Stiffness		Ultimate Moment	
		Experimental value (kN · m/rad) (3)	Percent change ^a (4)	Experimental value (kN · m) (5)	Percent change ^a (6)
<i>t</i>	Test 6, test 5	21,831; 48,445	+122%	92.00, 138.00	+50%
<i>t</i>	Test 7, test 8	79,936; 60,238	-25%	146.00, 102.00	-30%
<i>d_b</i>	Test 1, test 5	27,913; 48,445	+74%	89.00, 138.00	+55%
<i>d_b</i>	Test 4, test 12	20,068; 21,481	+7%	84.00, 104.00	+24%
<i>d_b</i>	Test 9, test 12	27,098; 21,481	-21%	132.00, 104.00	-21%
<i>g_c</i>	Test 11, test 12	71,089; 21,481	-70%	202.00, 104.00	-49%
<i>l_v</i>	Test 10, test 11	68,057; 71,089	+4%	188.00, 202.00	+7%
<i>d</i>	Test 6, test 8	21,831; 60,238	+176%	92.00, 102.00	+11%
<i>d</i>	Test 3, test 4	19,063; 20,068	+5%	95.00, 84.00	-12%
<i>d</i>	Test 5, test 8	48,445; 60,238	+24%	138.00, 102.00	-26%

^a+ sign indicates increase and - sign indicates decrease with respect to lower value reported in column to left.

“pinching” at higher load levels (refer to Fig. 3 for four test results). Pinching is characterized by an increase in rotation without a significant increase in moment, thus resulting in a loss in stiffness of the connection. In the top and seat angle connection, pinching was observed to occur due to excessive separation of the top or seat angle from the column flange. When the angle leg separated from the column flange, the moment-rotation hysteresis plot was observed to become very flat (i.e., rotation increased without any significant increase in moment), until contact between the angle leg and column flange again occurred during the load reversal. Then, the moment-rotation plot showed that the connection started to once again resist moment, and the connection rotation increase was accompanied by a significant increase in moment. As discussed earlier, the behavior of the top and seat angle connection is characterized by the initial stiffness, K_i , and the ultimate capacity, M_u . It would be of interest to investigate the effect of the geometry-related variables, which were varied in the test program, on these two parameters. These comparisons are presented in Table 2. From the values presented in this table, the following interesting observations are made:

1. When the variable t is varied by itself, it is observed to have a significant effect on both K_i and M_u (compare results for test 6 with test 5). However, when results for test 7 and test 8 are compared, it appears that the effect on K_i is not that significant. This may be due to the fact that the experimental value reported for test 7 is in doubt, because of experimental error.
2. When the variable d_b is varied by itself, it is observed to have a significant effect on both K_i and M_u , but it appears that the magnitude of the effect may also depend on the value of the beam depth [compare results for test 1 with test 5, where $d = 360$ mm (14 in.), and test 4 with test 12, where $d = 400$ mm (16 in.)]. If g_c and d_b are simultaneously varied, the magnitude of the effect is observed to decrease (compare results for test 9 and test 12).
3. When the variable g_c is varied by itself, it is observed to have a significant effect on both K_i and M_u (compare results for test 11 with test 12).
4. When the variable l_v is varied by itself, it is found to not have a significant effect on both K_i and M_u (compare results for test 10 with test 11).
5. When the variable d is varied by itself, in some cases it is observed to have a significant effect on K_i , but not on M_u (compare results for test 6 with test 8). But when g_c is simultaneously varied with d , the effect on both K_i and M_u is not that significant (compare results for test 3 and test 4). Similarly, when t is simultaneously varied with d , the effect on both K_i and M_u is a bit larger, but is still not too great (compare results for test 5 with test 8).

The above observations indicate three things: A more detailed parametric study is needed to investigate the relative contribution of each geometric variable to the behavior of the connection; the effect of some geometric variables is coupled; and there are some geometric variables that do not affect the behavior at all and may be eliminated when developing analytical expressions describing the connection behavior.

The results for K_i and M_u presented in Table 1 clearly show that the test cases selected did include very stiff to flexible connections (with K_i varying from 8,248 kN · m/rad to 71,089 kN · m/rad), and very high to low moment capacity connections (with M_u varying from 25 kN · m to 202 kN · m), as was intended. It would be worthwhile to mention that it is not an easy task to obtain the value of initial stiffness from physical tests, as also reported for static load studies (Barakat and Chen 1991); usually a lower and upper bound are estimated based on loading history and precision of measuring rotation produced at very small load values. In cyclic tests, the plastic deformations are not recovered upon unloading, and this damage accumulates as the number of cycles increases. Particularly if the bolt shank yields, this cumulative damage results in a misfit in the connection, which alters the behavior significantly; often, pinching of the moment-rotation loops occurs. These observations clearly point out the need for conducting a more comprehensive test program for steel connections subjected to cyclic loads in order to develop more generalized models.

MOMENT-ROTATION HYSTERESIS ANALYTICAL MODELS

Types of Models Considered

Analytical models describing the moment-rotation hysteresis behavior of semirigid connections are needed for dynamic frame analysis computer programs, in which such connections can be modeled as discrete moment-rotation spring elements connecting the beam end to the column end. In the present paper, an attempt is made to idealize the actual observed moment-rotation hysteresis behavior obtained from testing by following four types of analytical models: bilinear, elastoplastic, Ramberg-Osgood, and modified bilinear. The analytical moment versus rotation hysteresis variations for these four mathematical models are presented in Fig. 4. As can be seen in this figure, the bilinear and elastoplastic models belong to one class. Both of the models idealize the actual moment-rotation hysteresis behavior, but to varying degrees of accuracy. They also vary in level of complexity, as far as their implementation in a dynamic frame analysis computer program is concerned. The bilinear model is more accurate in modeling the moment-rotation behavior of the connection, whereas the elastoplastic model is more simple to implement in a frame analysis com-

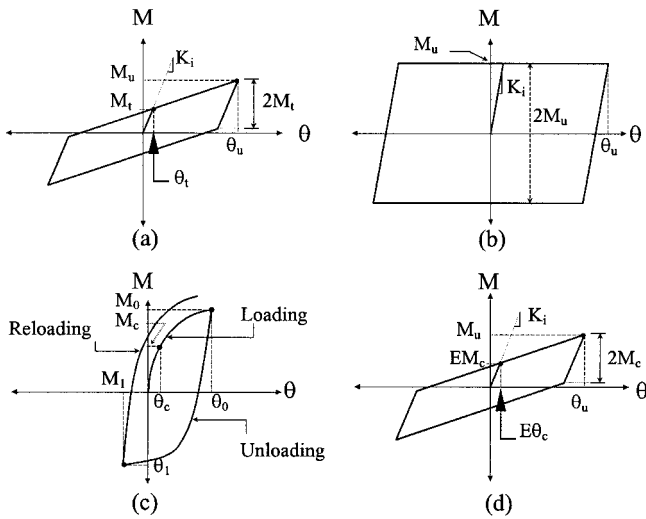


FIG. 4. Moment Rotation Mathematical Models: (a) Bilinear; (b) Elastoplastic; (c) Ramberg-Osgood; (d) Modified Bilinear

puter program. Thus, both of these models have their own merits. The bilinear model, as shown in Fig. 4(a), is defined by four parameters, which are the initial stiffness, K_i ; ultimate moment capacity, M_u ; ultimate rotation, θ_u ; and transition moment, M_t . The transition moment M_t is defined as the moment where the tangent line drawn from the point with coordinates (M_u, θ_u) and touching the enveloping moment-rotation curve (i.e., the curve passing through most of the peaks of the moment-rotation loops) intersects the initial stiffness slope line drawn at the origin. The elastoplastic model is a special case of the bilinear model, and, as shown in Fig. 4(b), it is described by only three parameters, K_i , M_u , and θ_u .

A typical moment-rotation loop for the Ramberg-Osgood analytical model, as shown in Fig. 4(c), consists of three non-linear portions, a loading, an unloading (at some known moment level), and a reloading path. Ramberg and Osgood (1943) have proposed equations for these curves. The relationship for loading is expressed mathematically as follows:

$$\frac{\theta}{\theta_c} = \frac{M}{M_c} \left(1 + \left| \frac{M}{M_c} \right|^{r-1} \right) \quad (1)$$

where θ = rotation corresponding to the applied moment, M ; θ_c = characteristic rotation; M_c = characteristic moment; r = rigidity parameter; and $| \cdot |$ denotes an absolute value. It should be noted that $r = 1$ denotes the least ductile connection, and $r = \infty$ represents the most ductile connection. The relationship for unloading takes the following form:

$$\frac{(\theta - \theta_0)}{2\theta_c} = \frac{(M - M_0)}{2M_c} \left[1 + \left| \frac{(M - M_0)}{2M_c} \right|^{r-1} \right] \quad (2)$$

where $\theta_0 = \theta$ -coordinate at the instant of unloading; and $M_0 = M$ -coordinate at the instant of unloading. Finally, the equation of the reloading portion takes the following form:

$$\frac{(\theta + \theta_1)}{2\theta_c} = \frac{(M - M_1)}{2M_c} \left[1 + \left| \frac{(M + M_1)}{2M_c} \right|^{r-1} \right] \quad (3)$$

where $\theta_1 = \theta$ -coordinate at the instant of reloading; and $M_1 = M$ -coordinate at the instant of reloading. The Ramberg-Osgood function, as defined by (1)–(3), cannot model the pinching portion of the moment-rotation curve; hence, it is used in the study to model only nonpinching regions of moment-rotation hysteresis curves (early load stages). The Ramberg-Osgood analytical model is the most complex in implementation out of the four models shown in Fig. 4, but is expected to be the most accurate to describe nonpinching behavior. It requires three parameters, which are M_c , θ_c , and r . The values of these three parameters that best fit the nonpinching loops of the 11 tests (test 7 is omitted), using the method of least squares, are presented in Table 3.

The modified bilinear model is selected by first fitting a Ramberg-Osgood model [(1)] through the experimental enveloping curve for the loading portion of the moment-rotation hysteresis loops. The experimental enveloping curve is defined as the curve passing through the peak points of each moment-rotation hysteresis loop in the positive quadrant only. The Ramberg-Osgood parameters of this enveloping curve (loading portion only) are denoted as EM_c , $E\theta_c$, and Er . The values of these three parameters that best fit the nonpinching loops of the 11 tests (test 7 is omitted), using the method of least squares, are presented in Table 4. Finally, the modified bilinear model, shown in Fig. 4(d), is defined in the same way as the bilinear model, shown in Fig. 4(a), except instead of using the

TABLE 3. Values Obtained for Ramberg-Osgood Parameters for Test Cases

Test number (1)	Test designation (2)	Ramberg-Osgood Parameter Values for Nonpinching Loops		
		M_c kN·m (kip-in.) (3)	θ_c (rad) (4)	r (5)
1	TS - 152 × 102 × 19 - 16 - 64 - 360 (TS - 6 × 4 × 3/4 - 5/8 - 2.5 - 14)	13.01 (115.15)	0.000245	1.58
2	TS - 152 × 152 × 9.5 - 16 - 114 - 360 (TS - 6 × 6 × 3/8 - 5/8 - 4.5 - 14)	13.55 (119.93)	0.004221	3.56
3	TS - 152 × 152 × 19 - 16 - 90 - 360 (TS - 6 × 6 × 3/4 - 5/8 - 3.5 - 14)	35.00 (307.78)	0.001288	1.30
4	TS - 152 × 152 × 19 - 16 - 114 - 400 (TS - 6 × 6 × 3/4 - 5/8 - 4.5 - 16)	24.00 (212.43)	0.000700	1.30
5	TS - 152 × 102 × 19 - 19 - 64 - 360 (TS - 6 × 4 × 3/4 - 3/4 - 2.5 - 14)	20.00 (177.022)	0.000221	1.49
6	TS - 152 × 102 × 12.7 - 19 - 64 - 360 (TS - 6 × 4 × 1/2 - 3/4 - 2.5 - 14)	28.25 (251.81)	0.001112	2.83
8	TS - 152 × 102 × 12.7 - 19 - 64 - 400 (TS - 6 × 4 × 1/2 - 3/4 - 2.5 - 16)	24.86 (220.00)	0.000520	2.62
9	TS - 152 × 152 × 19 - 19 - 90 - 400 (TS - 6 × 6 × 3/4 - 3/4 - 3.5 - 16)	32.00 (283.23)	0.000710	1.52
10	TS - 152 × 102 × 19 - 22 - 64 - 400 (TS - 6 × 4 × 3/4 - 7/8 - 2.5 - 16)	56.49 (500)	0.000538	1.55
11	TS - 152 × 152 × 19 - 22 - 64 - 400 (TS - 6 × 6 × 3/4 - 7/8 - 2.5 - 16)	28.00 (247.83)	0.000239	1.60
12	TS - 152 × 152 × 19 - 22 - 114 - 400 (TS - 6 × 6 × 3/4 - 7/8 - 4.5 - 16)	22.01 (194.84)	0.000621	1.37

TABLE 4. Values Obtained for Ramberg-Osgood Parameters Enveloping Curve for Test Cases

Test Number (1)	Test designation (2)	Ramberg-Osgood Parameter Values		
		EM_c kN·m (kip-in.) (3)	$E\theta_c$ (rad) (4)	E_r (5)
1	TS – 152 × 102 × 19 – 16 – 64 – 360 (TS – 6 × 4 × 3/4 – 5/8 – 2.5 – 14)	36.60 (324.0)	0.002465	2.30
2	TS – 152 × 152 × 9.5 – 16 – 114 – 360 (TS – 6 × 6 × 3/8 – 5/8 – 4.5 – 14)	14.68 (124.0)	0.004221	4.50
3	TS – 152 × 152 × 19 – 16 – 90 – 360 (TS – 6 × 6 × 3/4 – 5/8 – 3.5 – 14)	39.54 (345)	— ^a	— ^a
4	TS – 152 × 152 × 19 – 16 – 114 – 400 (TS – 6 × 6 × 3/4 – 5/8 – 4.5 – 16)	56.49 (500)	0.003571	5.97
5	TS – 152 × 102 × 19 – 19 – 64 – 360 (TS – 6 × 4 × 3/4 – 3/4 – 2.5 – 14)	61.00 (540)	0.003771	2.93
6	TS – 152 × 102 × 12.7 – 19 – 64 – 360 (TS – 6 × 4 × 1/2 – 3/4 – 2.5 – 14)	47.45 (422.64)	0.003801	3.55
8	TS – 152 × 102 × 12.7 – 19 – 64 – 400 (TS – 6 × 4 × 1/2 – 3/4 – 2.5 – 16)	56.49 (500)	0.003883	3.97
9	TS – 152 × 152 × 19 – 19 – 90 – 400 (TS – 6 × 6 × 3/4 – 3/4 – 3.5 – 16)	53.78 (476)	0.002303	3.14
10	TS – 152 × 102 × 19 – 22 – 64 – 400 (TS – 6 × 4 × 3/4 – 7/8 – 2.5 – 16)	82.02 (726)	0.003237	2.82
11	TS – 152 × 152 × 19 – 22 – 64 – 400 (TS – 6 × 6 × 3/4 – 7/8 – 2.5 – 16)	56.49 (500)	0.002435	2.07
12	TS – 152 × 152 × 19 – 22 – 114 – 400 (TS – 6 × 6 × 3/4 – 7/8 – 4.5 – 16)	58.52 (518)	0.003084	4.35

^aA reliable value could not be determined for this test.

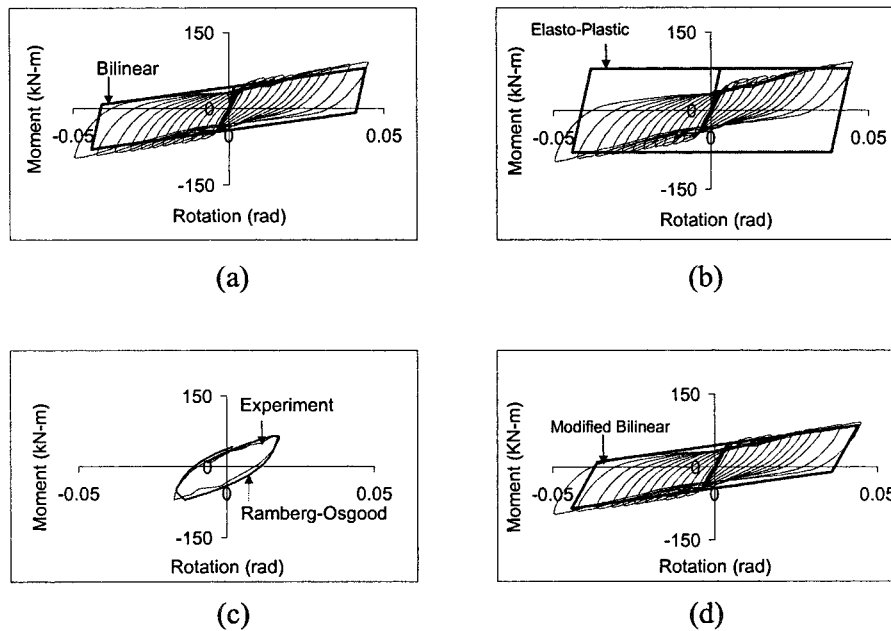


FIG. 5. Comparison of Model Moment-Rotation Behavior with Experimental Hysteresis Loops for Test 6 (TS – 152 × 102 × 12.7 – 19 – 64 – 360): (a) Bilinear; (b) Elastoplastic; (c) Ramberg-Osgood; (d) Modified Bilinear

transition point with coordinates (M_i, θ_i) , the characteristic point with coordinates $(EM_c, E\theta_c)$ is used. Thus, this model is characterized by the following four parameters: EM_c , $E\theta_c$, M_i , and θ_i . It would be of interest to see how these model predictions compare with those obtained from the previous bilinear model.

Regression Analysis

A nonlinear regression analysis of the test results was conducted to obtain prediction equations for the parameters described for the four moment-rotation hysteresis models shown in Fig. 5, which are K_i , M_i , θ_i , M_c , θ_c , r , EM_c , and $E\theta_c$. Prediction equations for these parameters (dependent variables) are obtained in terms of the connection geometry and

force-related variables (independent variables). The connection geometric variables were defined earlier, as shown in Fig. 1. These independent geometric variables are normalized with respect to the angle length, l_v , to define the following independent nondimensional parameters: g_c/l_v , t/l_v , b_d/l_v , d/l_v , g_c/l_v , and $g_c t^2/l_v^3$. During testing, it was observed in all tests that as the beam end rotated, the angle leg bolted to the column flange behaved as a cantilever beam with a span equal to g_c (=distance between the first bolt row and the heel of the angle), depth equal to t (=angle thickness), and width equal to unity. This cantilever was pulled by the beam flange force created due to the moment acting on the beam end. The last independent parameter, $g_c t^2/l_v^3$, is added to account for this bending behavior of the angle leg of the top and seat angle, which is bolted to the column flange. When developing the best pre-

dition equations for the dependent parameters, it was found that different forms (not necessarily nondimensional) of force-related independent parameters gave better prediction equations for different dependent parameters. For K_i , M_u , M_t , and M_c , the force-related independent parameter that best fit the test data was found to be F_y/l_v , where F_y is the yield stress (obtained from uniaxial coupon tension tests) of the angle material. Similarly, for M_c and $E\theta_c$, the best force-related independent parameter was found to be M_u/θ_u ; for θ_c , the best force-related independent parameter was found to be M_c ; and for $E\theta_c$, the best force-related independent parameter was found to be M_c/l_v . These were all obtained by trial and error. It should be noted that in developing these prediction equations, the yield stress, F_y , of the angle material was considered as a variable, because its incorporation produced better results. The bolt material yield stress was not considered as a variable. Based on tensile coupon tests conducted on the material used for each type of angle, some variation in the values of F_y was observed; those values are presented in the third column of Table 1. The writers do not imply that the equations reported in the present paper should be used for different steel grades, where F_y may vary significantly from the values shown in Table 1. More experimental tests are needed with specimens of other steel grades in order to develop general equations in which F_y can be truly treated as a variable.

A prediction equation for a dependent variable obtained from the nonlinear regression analysis of the test results was considered to be acceptable if its value of $R^2 > 0.90$, where R^2 is the coefficient of multiple regression [a value of $R^2 = 0.9$ means that 90% of the sum of the squares of the deviation of the observed values (experimental values, which are input) about their mean can be explained by the prediction equation]. Next, a scatter plot of the actual (observed value obtained from test results) versus the predicted (obtained from the prediction equation) values was developed for each prediction equation. In this plot, three lines were also drawn with the following slopes (vertical:horizontal): 1:1, 1.2:1, and 1:0.8. A data point lying on the 1:1 slope line shows that this data point satisfies the prediction equation exactly, whereas if it lies on the 1.2:1 or 0.8:1 line, it differs from the predicted value by +20% (i.e., greater) or -20% (i.e., smaller), respectively. Thus, the 1.2:1 and 0.8:1 slope lines indicate an error band of +20% and -20%, which was considered to be the acceptable band, to start with, in the present study. If any data point fell outside this error band, that point was removed, and the regression analysis was repeated with the hope of obtaining a better prediction equation (i.e., with an improved R^2). If R^2 decreased by removing this point from the regression analysis, then that point was not removed, and the prediction equation was reported with a higher error band.

After obtaining the best prediction equation for a dependent parameter following the above procedure, a sensitivity study was conducted to check if the prediction equation showed a similar trend when a geometric variable was varied, as was observed from tests. To evaluate the effect of each independent geometric variable on the dependent parameter, one at a time, this variable was varied from low to intermediate to high values while holding the value of all of the other geometric variables at their intermediate value. Graphical plots showing the variation of the dependent variable versus each independent variable were obtained to ascertain the following two points: Is the variation consistent with that observed from experimental tests? Is the effect of the independent variable significant (e.g., if a flat or close to a horizontal curve was obtained, it indicated that independent variable did not significantly affect the dependent variable)? Independent variables that were found to not contribute significantly to the dependent variable prediction were then dropped, and in the regression analysis

was repeated to obtain a simplified prediction equation, but it was checked that the R^2 did not decrease. The sensitivity study indicated the following: (1) The geometric variables g_c , t , d_b , and d have a significant effect on K_i ; however, when d and g_c are both simultaneously increased, the combined effect on K_i is insignificant, because decreasing d increases K_i and increasing g_c decreases K_i , and the two effects neutralize each other; (2) the geometric variable l_v does not significantly affect K_i ; (3) the geometric variables g_c and t have a significant effect on M_u ; (4) the geometric variable d_b has a moderate effect on M_u ; and (5) the geometric variables l_v and d do not significantly affect M_u .

Using the aforementioned regression analysis procedure, the prediction equations obtained, in the International System of Units, including their corresponding R^2 and error band, for the model parameters are as follows:

$$K_i = 8,633.178 \left(\frac{g_c}{l_v}\right)^{13.0772} \left(\frac{t}{l_v}\right)^{30.4653} \left(\frac{d_b}{l_v}\right)^{0.3648} \left(\frac{d}{l_v}\right)^{3.5029} \cdot \left(\frac{g_b}{l_v}\right)^{0.2993} \left(\frac{g_c t^2}{l_v^3}\right)^{-15.0471} \left(\frac{F_y}{l_v}\right)^{-2.1580};$$

$$(R^2 = 0.97; \text{ error band} = +23\% \text{ to } -24\%) \quad (4)$$

$$M_u = 2,017.68 \left(\frac{g_c}{l_v}\right)^{23.737} \left(\frac{t}{l_v}\right)^{51.073} \left(\frac{d_b}{l_v}\right)^{0.7700} \cdot \left(\frac{g_b}{l_v}\right)^{-1.2498} \left(\frac{g_c t^2}{l_v^3}\right)^{-24.9388} \left(\frac{F_y}{l_v}\right)^{0.2077};$$

$$(R^2 = 0.96; \text{ error band} = +23\% \text{ to } -13\%) \quad (5)$$

$$\theta_u = 1,539.87 \left(\frac{g_c}{l_v}\right)^{-67.8437} \left(\frac{t}{l_v}\right)^{-142.26} \left(\frac{d_b}{l_v}\right)^{-0.89193} \left(\frac{d}{l_v}\right)^{-1.1639} \cdot \left(\frac{g_b}{l_v}\right)^{-0.17089} \left(\frac{g_c t^2}{l_v^3}\right)^{70.7078} \left(\frac{F_y g_c t}{M_u}\right)^{-1.35491};$$

$$(R^2 = 0.98; \text{ error band} = +5\% \text{ to } -5\%) \quad (6)$$

$$M_t = 141.189 \left(\frac{g_c}{l_v}\right)^{21.4920} \left(\frac{t}{l_v}\right)^{46.3482} \left(\frac{d_b}{l_v}\right)^{-0.2833} \cdot \left(\frac{g_b}{l_v}\right)^{-1.4535} \left(\frac{g_c t^2}{l_v^3}\right)^{-22.4276} \left(\frac{F_y}{l_v}\right)^{1.08207};$$

$$(R^2 = 0.93; \text{ error band} = +18\% \text{ to } -21\%) \quad (7)$$

$$M_c = 8.53111 \times 10^6 \left(\frac{g_c}{l_v}\right)^{-4.45815} \left(\frac{t}{l_v}\right)^{-1.11129} \left(\frac{d_b}{l_v}\right)^{0.4678} \left(\frac{g_b}{l_v}\right)^{-2.3970} \cdot \left(\frac{g_c t^2}{l_v^3}\right)^{2.1206} \left(\frac{F_y}{l_v}\right)^{1.6337} \left(\frac{M_u}{\theta_u}\right)^{-0.70267};$$

$$(R^2 = 0.99; \text{ error band} = +5\% \text{ to } -5\%) \quad (8)$$

$$\theta_c = 2.59 \times 10^{-7} \left(\frac{g_c}{l_v}\right)^{4.2664} \left(\frac{t}{l_v}\right)^{2.2766} \left(\frac{d_b}{l_v}\right)^{-0.7220} \left(\frac{d}{l_v}\right)^{-0.99207} \cdot \left(\frac{g_b}{l_v}\right)^{1.8087} \left(\frac{g_c t^2}{l_v^3}\right)^{-2.3486} (M_c)^{1.1555};$$

$$(R^2 = 0.97; \text{ error band} = +28\% \text{ to } -20\%) \quad (9)$$

$$r = 0.110658 \left(\frac{g_c}{l_v}\right)^{-8088.10} \left(\frac{t}{l_v}\right)^{-161766} \left(\frac{d_b}{l_v}\right)^{-1.02919} \left(\frac{d}{l_v}\right)^{0.482055} \cdot \left(\frac{g_b}{l_v}\right)^{-0.00295} \left(\frac{g_c t^2}{l_v^3}\right)^{8088.23} \left(\frac{M_c}{l_v}\right)^{0.6929};$$

$$(R^2 = 0.97; \text{ error band} = +17\% \text{ to } -15\%) \quad (10)$$

$$EM_c = 115.303 \left(\frac{g_c}{l_v}\right)^{-0.71197} \left(\frac{t}{l_v}\right)^{-0.09605} \left(\frac{b_d}{l_v}\right)^{-0.01402} \cdot \left(\frac{g_b}{l_v}\right)^{-1.51273} \left(\frac{g_c t^3}{l_v^3}\right)^{0.697946} \left(\frac{F_y}{l_v}\right)^{1.61499};$$

$(R^2 = 0.98; \text{ error band} = +11\% \text{ to } -11\%)$ (11)

$$E\theta_c = 6.5380 \times 10^{22} \left(\frac{g_c}{l_v}\right)^{-14.3806} \left(\frac{t}{l_v}\right)^{-10.411} \left(\frac{b_d}{l_v}\right)^{2.6303} \left(\frac{d}{l_v}\right)^{-0.9885} \cdot \left(\frac{g_b}{l_v}\right)^{-2.736} \left(\frac{g_c t^2}{l_v^3}\right)^{9.1619} \left(\frac{M_u}{\theta_u}\right)^{-4.9617};$$

$(R^2 = 0.98; \text{ error band} = +5\% \text{ to } -5\%)$ (12)

It should be noted that the results presented in Table 3 are used to obtain (8) and (9), and the results presented in Table 4 are used to obtain (10)–(12). In all of the prediction equations, the geometric variables are to be substituted in millimeter units, and the moments, in kN·m units. The values obtained for K_i , M_u , θ_u , M_t , M_c , θ_c are in kN·m/rad, kN·m, rad, kN·m, kN·m, and rad units, respectively. The parameter r is a scalar number. The corresponding prediction equations [corresponding to (4)–(12), respectively] obtained in U.S. customary units for the model parameters are as follows:

$$K_i = 12,742.38 \left(\frac{g_c}{l_v}\right)^{-9.1973} \left(\frac{t}{l_v}\right)^{-14.0835} \left(\frac{b_d}{l_v}\right)^{0.3648} \left(\frac{d}{l_v}\right)^{3.5029} \cdot \left(\frac{g_b}{l_v}\right)^{-0.2993} \left(\frac{g_c t^2}{l_v^3}\right)^{7.2273} \left(\frac{F_y}{l_v}\right)^{-2.1580}$$
 (13)

$$M_u = 13,621.57 \left(\frac{g_c}{l_v}\right)^{-5.8805} \left(\frac{t}{l_v}\right)^{-8.1612} \left(\frac{b_d}{l_v}\right)^{0.7696} \left(\frac{g_b}{l_v}\right)^{-1.2498} \cdot \left(\frac{g_c t^2}{l_v^3}\right)^{4.6786} \left(\frac{F_y}{l_v}\right)^{0.2077}$$
 (14)

$$M_t = 304.79 \left(\frac{g_c}{l_v}\right)^{-1.9861} \left(\frac{t}{l_v}\right)^{-0.6081} \left(\frac{b_d}{l_v}\right)^{-0.2833} \left(\frac{g_b}{l_v}\right)^{-1.4535} \cdot \left(\frac{g_c t^2}{l_v^3}\right)^{1.0505} \left(\frac{F_y}{l_v}\right)^{1.08207}$$
 (15)

$$\theta_u = 9.15 \times 10^{-4} \left(\frac{g_c}{l_v}\right)^{5.9077} \left(\frac{t}{l_v}\right)^{5.2429} \left(\frac{b_d}{l_v}\right)^{-0.89193} \left(\frac{d}{l_v}\right)^{-1.1639} \cdot \left(\frac{g_b}{l_v}\right)^{-0.17089} \left(\frac{g_c t^2}{l_v^3}\right)^{-3.04364} \left(\frac{F_y g_c t}{M_u}\right)^{-1.35491}$$
 (16)

$$M_c = 8.53111 \times 10^6 \left(\frac{g_c}{l_v}\right)^{-4.4581} \left(\frac{t}{l_v}\right)^{-1.11129} \left(\frac{b_d}{l_v}\right)^{0.4678} \left(\frac{G_b}{l_v}\right)^{-2.397} \cdot \left(\frac{g_c t^2}{l_v^3}\right)^{2.1206} \left(\frac{F_y}{l_v}\right)^{1.6337} \left(\frac{M_u}{\theta_u}\right)^{-0.70267}$$
 (17)

$$\theta_c = 2.10 \times 10^{-8} \left(\frac{g_c}{l_v}\right)^{5.0983} \left(\frac{t}{l_v}\right)^{3.9406} \left(\frac{b_d}{l_v}\right)^{-0.7220} \left(\frac{d}{l_v}\right)^{-0.99207} \cdot \left(\frac{g_b}{l_v}\right)^{1.8087} \left(\frac{g_c t^2}{l_v^3}\right)^{-3.1806} (M_c)^{1.1555}$$
 (18)

$$r = 0.0026 \left(\frac{g_c}{l_v}\right)^{-82715.2} \left(\frac{t}{l_v}\right)^{-165434} \left(\frac{b_d}{l_v}\right)^{-1.02951} \left(\frac{d}{l_v}\right)^{0.481887} \cdot \left(\frac{g_b}{l_v}\right)^{-0.00282} \left(\frac{g_c t^2}{l_v^3}\right)^{82716.42} \left(\frac{M_c}{l_v}\right)^{0.693153}$$
 (19)

$$EM_c = 124.237 \left(\frac{g_c}{l_v}\right)^{-0.56203} \left(\frac{t}{l_v}\right)^{0.203834} \left(\frac{b_d}{l_v}\right)^{-0.01402} \left(\frac{g_b}{l_v}\right)^{-1.51273} \cdot \left(\frac{g_c t^3}{l_v^3}\right)^{0.548} \left(\frac{F_y}{l_v}\right)^{1.6150}$$
 (20)

$$E\theta_c = 3.2675 \times 10^{27} \left(\frac{g_c}{l_v}\right)^{-7.8714} \left(\frac{t}{l_v}\right)^{2.6075} \left(\frac{b_d}{l_v}\right)^{2.6303} \left(\frac{d}{l_v}\right)^{-0.9985} \cdot \left(\frac{g_b}{l_v}\right)^{-2.736} \left(\frac{g_c t^2}{l_v^3}\right)^{2.65266} \left(\frac{M_u}{\theta_u}\right)^{-4.9617}$$
 (21)

It should be noted that the results presented in Table 3 are used to obtain (17) and (18), and the results presented in Table 4 are used to obtain (19)–(21). In all of the prediction equations, the geometric variables are to be substituted in inch units, and moments, in kip-in. units. The values obtained for K_i , M_u , θ_u , M_t , M_c , θ_c are in kip-in./rad, kip-in., rad, kip-in., kip-in., and rad units, respectively.

Validation of Parameter Prediction Equations and Models Developed

To validate the parametric prediction equations and the hysteresis models developed, the experimental moment-rotation hysteresis loops are plotted and compared with the mathematical bilinear, elastoplastic, Ramberg-Osgood, and modified bilinear Ramberg-Osgood models, and the results obtained for only one test (test 6) are presented in Fig. 5; similar results were obtained for other test cases. From these plots, it can be seen that the different models idealize the experimental moment-rotation loops to different degrees of accuracy. Overall, the elastoplastic model is the least conservative [Fig. 5(b)]; the modified bilinear model predictions are the best [Fig. 5(d)] and are an improvement over the conventional bilinear model [Fig. 5(a)]. As stated earlier, the Ramberg-Osgood model is only applicable for nonpinching moment-rotation loops; these loops are very accurately predicted by this model, as can be seen in Fig. 5(c). In this plot, the experimental and predicted plots basically overlapped one another, so only one loop is presented in Fig. 5(c). For the modified bilinear model, the enveloping curve for each test is used to compute the Ramberg-Osgood parameters, and these values, which were presented in Table 4, were regressed to develop prediction equations for EM_c and $E\theta_c$. Also, a prediction equation was developed for Er , which is not presented in the current paper. Using these prediction equations for these three Ramberg-Osgood parameters (i.e., for EM_c , $E\theta_c$, and Er), a predicted moment-rotation enveloping curve can be plotted for each test case and compared to that obtained from experimental results to validate the prediction capabilities of these prediction equations. The plots obtained for four tests (tests 2, 6, 5, and 11) are presented in Fig. 6; similar plots were obtained for other test cases. These plots do show that the prediction equations developed for EM_c and $E\theta_c$ predict results that compare well with the experimental results.

The modified bilinear model, which uses the characteristic moment M_c , instead of the arbitrarily chosen transition moment M_t , was suggested with the expectation that it would idealize better the actual moment-rotation behavior. Comparing the results presented in Figs. 5(a) and 5(d) for test 6, this is observed to be true. To further validate this observation, a comparison of the experimental moment-rotation hysteresis loops recorded for four other tests (tests 2, 6, 5, and 10) with

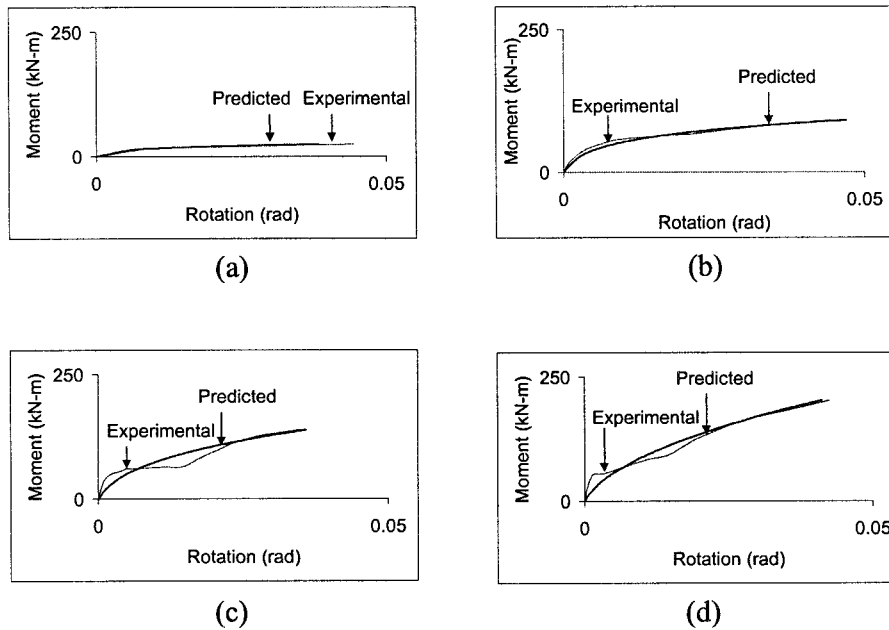


FIG. 6. Comparison of Experimental and Modified Bilinear Predicted Curves: (a) Test 2: $TS - 152 \times 152 \times 9.5 - 16 - 114 - 356$; (b) Test 6: $TS - 152 \times 102 \times 12.7 - 19 - 64 - 360$; (c) Test 5: $TS - 152 \times 102 \times 19 - 19 - 64 - 360$; (d) Test 11: $TS - 152 \times 152 \times 19 - 22 - 64 - 400$

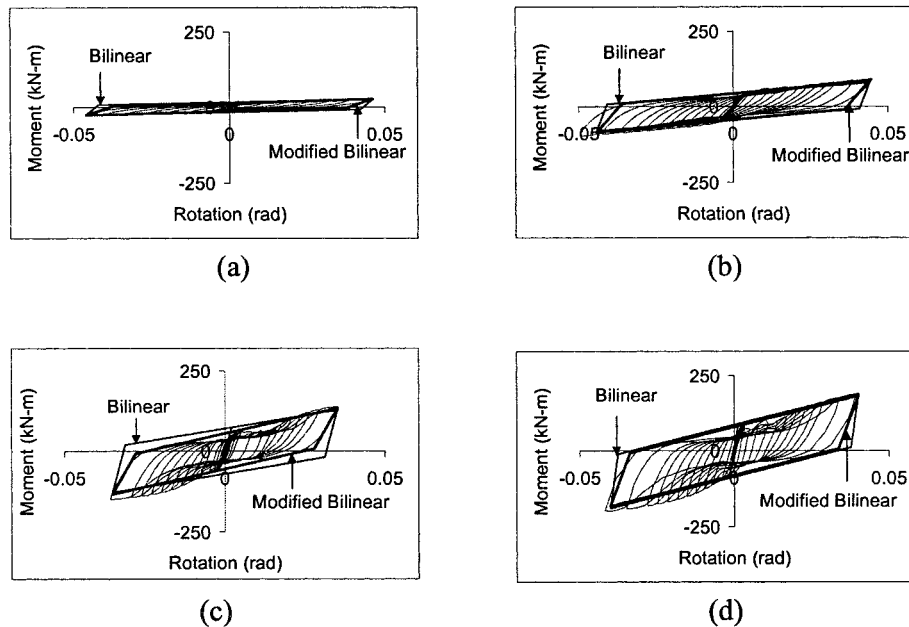


FIG. 7. Comparison of Bilinear and Modified Bilinear with Experimental Hysteresis Loops for: (a) Test 2: $TS - 152 \times 152 \times 9.5 - 16 - 114 - 360$; (b) Test 6: $TS - 152 \times 102 \times 12.7 - 19 - 64 - 360$; (c) Test 5: $TS - 152 \times 102 \times 19 - 19 - 64 - 360$; (d) Test 10: $TS - 152 \times 102 \times 19 - 22 - 64 - 400$

the bilinear and the modified bilinear models is shown in Fig. 7. The results presented in Fig. 7 show that the modified bilinear model is an improvement over the conventional bilinear model.

CONCLUSIONS

The top and seat angle connection behaves as a semirigid connection. A wide range of initial stiffnesses, K_i , and ultimate moment capacities, M_u , are possible to achieve by altering the connection geometry related variables within a practical range. For certain geometric configurations of the connection, significant transfer of moment from the beam to the column can occur before the connection fails. Also, it is possible to design a connection with low stiffness and small moment transfer

capability, so that it behaves in a way whereby it is close to being classified as a pin connection.

For the top and seat steel framing connection, the parameters that define the variation of the moment-rotation hysteresis loops for the bilinear, elastoplastic, Ramberg-Osgood, and modified bilinear analytical models have been identified, and prediction equations for each have been developed using test results. It has been shown that these prediction equations and the four hysteresis models presented give acceptable results when compared to experimental results. The degree to which the models idealize the actual behavior varies with the elastoplastic model being the least conservative, and the modified bilinear model being the best. The Ramberg-Osgood model is the most accurate in just modeling the nonpinching moment-rotation loops. The modified bilinear model, which uses the

characteristic moment, EM_c , instead of the transition moment, M_t , used in the conventional bilinear model, predicts better results. It is expected that the elastoplastic model would be the simplest to implement in a base motion (dynamic) finite-element frame analysis computer program; the bilinear model and the modified bilinear model would not be significantly difficult to implement also. However, the Ramberg-Osgood model would be the most complex, and would require an iterative procedure to march along the nonlinear moment-rotation curve. These observations still have to be verified. Finally, in the present paper, an approach to develop analytical models describing the hysteresis behavior of the top and seat angle connection is presented using results from only 12 test data. A more comprehensive study needs to be undertaken, in which more cases are considered to incorporate other possible variations before generalizations can be made.

ACKNOWLEDGMENTS

The writers would like to acknowledge the help given by Arnaud Bastide, foreign exchange undergraduate student from C.U.S.T., University of Blaise Pascal, Clermont, France, who assisted in fabricating the connection specimens and in conducting the tests during his study at the University of Oklahoma from January to June 1997.

APPENDIX I. REFERENCES

- Astaneh-Asl, A., Nader, M. N., and Malik, L. (1989). "Cyclic behavior of double angle connections." *J. Struct. Engrg.*, ASCE, 115(5), 1101–1118.
- Barakat, M., and Chen, W. F. (1991). "Design analysis of semi-rigid frames: Evaluation and implementation." *Engrg. J.*, 28(2), 55–64.
- Biolzi, L. (1992). "Discussion of 'Cyclic behavior of end-plate moment connections,' by Keh-Chyuan Tsai and Egor P. Popov." *J. Struct. Engrg.*, ASCE, 118(3), 874–877.
- Driscoll, G. C., and Lu, L. W. (1989). "Top and seat angle connections and end-plate connections: Snug versus fully pretensioned bolts." *ATLSS Rep. No. 89-06 Prepared for Nat. Sci. Found.*, Lehigh University, Bethlehem, Pa.
- Hechtman, R. A., and Johnston, B. G. (1947). "Riveted semi-rigid beam-to-column building connection." *Progress Rep. No. 1 Prepared for Am. Inst. of Steel Constr.*, Lehigh University, Bethlehem, Pa.
- Kishi, N., and Chen, W. F. (1986). "Steel construction data bank program." *Struct. Engrg. Rep. No. CE-STR-86-18*, School of Civil Engineering, Purdue University, West Lafayette, Ind.
- Kishi, N., and Chen, W. F. (1987a). "Moment rotation of top and seat angle connections." *Struct. Engrg. Rep. No. CE-STR-87-4*, School of Civil Engineering, Purdue University, West Lafayette, Ind.
- Kishi, N., and Chen, W. F. (1987b). "Moment rotation of top and seat angle connections." *Struct. Engrg. Rep. No. CE-STR-87-29*, School of Civil Engineering, Purdue University, West Lafayette, Ind.
- Lee, S. J., and Lu, L. (1988). "Cyclic test of full scale composite joint assemblages." *J. Struct. Engrg.*, ASCE, 115(8), 1977–1998.
- Mander, J. B., Chen, S. S., and Pekan, G. (1994). "Low-cycle fatigue behavior of semi-rigid top-and-seat angle connections." *Engrg. J.*, 31(3), 111–122.
- Manual of steel construction: Load and resistance factor design: Volume 2*, 2nd Ed. (1994). American Institute of Steel Construction, Chicago.
- Marley, M. J., and Gerstle, K. H. (1982). "Analysis and tests of flexibil-

- ity-connected steel frames." *Rep. for Proj. No. 199 Prepared for Am. Inst. of Steel Constr.*, University of Colorado, Boulder.
- Nader, M. N., and Astaneh-Asl, A. (1996). "Shaking table tests of rigid, semirigid, and flexible steel frames." *J. Struct. Engrg.*, ASCE, 122(6), 589–596.
- Popov, E. P., Amin, N. R., Louie, J. C., and Stephen, R. M. (1985). "Cyclic behavior of large beam-column assemblages." *Earthquake Spectra*, 1(2), 201–237.
- Popov, E. P., and Bertero, V. V. (1973). "Cyclic loading of steel beams and connections." *J. Struct. Div.*, ASCE, 99(6), 1189–1204.
- Popov, E. P., and Pinkey, R. B. (1968). "Cyclic loading of steel beams and connections subjected to inelastic strain reversals." *Bull. No. 3*, (Nov.), American Iron and Steel Institute, Washington, D.C.
- Ramberg, W., and Osgood, W. R. (1943). "Description of stress-strain curves by three parameters." *Monograph No. 4*, Pubblicazione Italsider, Nuova Italsider, Genova.
- Rathbun, J. C. (1936). "Elastic properties of riveted connections." *Paper No. 1933, Trans.*, ASCE, Reston, Va., 101, 524–563.
- Saraf, M., and Bruneau, M. (1996). "Cyclic testing of existing and retrofitted riveted stiffened seat angle connections." *J. Struct. Engrg.*, ASCE, 122(7), 762–775.
- Tsai, K. C. (1988). "Steel beam-column joint in seismic moment-resisting frames," MS thesis, University of California, Berkeley, Calif.
- Tsai, K. C., and Popov, E. P. (1990). "Cyclic behavior of end-plate moment connections." *J. Struct. Engrg.*, ASCE, 116(11), 2917–2930.
- Tsai, K. C., Wu, S., and Popov, E. P. (1995). "Experimental performance of seismic steel beam-column moment joints." *J. Struct. Engrg.*, ASCE, 116(6), 925–931.
- Vayas, L., Pasternak, H., and Schween, T. (1995). "Cyclic behavior of beam-to-column steel joints with slender web panels." *J. Struct. Engrg.*, ASCE, 121(2), 240–248.

APPENDIX II. NOTATION

The following symbols are used in this paper:

- d = beam depth;
 d_b = bolt diameter;
 EM_c = enveloping Ramberg-Osgood characteristic moment parameter;
 Er = enveloping Ramberg-Osgood rigidity parameter;
 $E\theta_c$ = enveloping Ramberg-Osgood characteristic rotation parameter;
 F_y = yield stress of angle material;
 g_b = gauge between bolts;
 g_c = distance from heel of angle to first row of bolts;
 K_i = initial stiffness of connection;
 l = angle length;
 l_h = length of horizontal angle leg;
 l_v = length of vertical angle leg;
 M_c = transition moment;
 M_t = transition moment;
 M_u = ultimate connection moment capacity;
 M_0 = M -coordinate at instant of unloading;
 M_1 = M -coordinate at instant of reloading;
 r = Ramberg-Osgood rigidity parameter;
 t = angle thickness;
 θ_u = Ramberg-Osgood characteristic rotation;
 θ_0 = θ -coordinate at instant of unloading; and
 θ_1 = θ -coordinate at instant of reloading.